# 5d-mediated indirect exchange and effective spin Hamiltonians in Ce triangular-lattice delafossites

Leonid V. Pourovskii<sup>1, 2, \*</sup>

<sup>1</sup>CPHT, CNRS, École polytechnique, Institut Polytechnique de Paris, 91120 Palaiseau, France <sup>2</sup>Collège de France, Université PSL, 11 place Marcelin Berthelot, 75005 Paris, France

Anisotropic intersite exchange interactions in frustrated rare-earth magnets are difficult to assess both theoretically and experimentally. Here, we propose an ab initio force-theorem framework combining the quasi-atomic Hubbard-I approach to 4f correlations with a static mean-field treatment of the on-site intershell Coulomb interaction between rare-earth 4f and 5d states to simultaneously capture both 4f superexchange and 5d-mediated indirect exchange. Applying it to the triangular lattice Ce delafossites CsCeSe<sub>2</sub>, KCeS<sub>2</sub>, and RbCeO<sub>2</sub>, we find that the indirect exchange dominates in the selenide, the superexchange in the oxide, while both mechanisms contribute almost equally in the sulfide. The magnetic exciation spectra of CsCeSe<sub>2</sub> and KCeS<sub>2</sub> evaluated from the calculated spin Hamiltonains are in good qualitative and quantitative agreement with experimental data.

Introduction. Rare-earth magnetism stems from the partually filled rare-earth (RE) 4f shells, where a strong spin-orbit coupling, weaker crystal-field (CF) effects and anisotropic intersite exchange interactions (IEI) intertwine to induce an enormous variety of magnetic phases. Those include a rich zoo of magnetic orders like, for example, incommensurate helical orders in heavy RE metals [1], ferromagnetic RE semiconductors [2], primary multipolar orders in the Ce hexaboride [3, 4], PrO<sub>2</sub> [5, 6], Pr "1-2-20" cage compounds [7], as well as even more exotic quantum spin liquid (QSL) phases. The latter are suspected to occur in RE pyrochlores [8–10] and in RE triangular-lattice lattice systems like the delafossites  $ARX_2$  (where R is a 3+ rare-earth ion, X is a ligand and A is a non-magnetic cation) [11] or the heptatantalates RTa<sub>7</sub>O<sub>19</sub> [12].

Apart from few possible exceptions like  $\alpha$ -Ce [13], direct hopping between 4f shells is believed to be negligible. IEI thus arise due to indirect 4f hopping through ligand states leading to superexchange, or due to indirect exchange involving the on-site Coulomb interaction between 4f and 5d states. Both mechanism are believed to contribute comparably in the Eu chalcogenides [2, 14], where the Eu<sup>2+</sup> ion possesses no orbital moment, simplifying the analysis of kinetic exchange processes. A more general case of both spin and orbital RE moment being non-zero forming a Hund's rule ground state (GS) in accordance with the LS coupling scheme is though far more common. In this case one may expect an essential IEI anisotropy as well as high-rank multipoles playing an important role in the case of a large CF GS degeneracy [5]. Few theoretical approaches are currently available to treat this general case [15–17], with their range of applicability not clearly understood [18].

The lack of quantitative theoretical approaches to evaluate intersite exchange in realistic RE systems is apparent in the case of RE delafossites  $ARX_2$  hosting a perfect triangular lattice of R=Ce, Yb ions. A strong CF on the R 4f shell leads to a pseudo-spin-1/2 Kramers

doublet GS that is energetically well isolated from exited CF levels. A Dirac QSL phase and its derivatives are suggested to occur in the spin-1/2 triangular lattice model for a certain range of IEI [19–26]. Experimentally, strong evidences for possible QSL phases were found in several Yb delafossites  $AYbX_2$  (A=K, Na and X=O, S, Se) [27–30]. In contrast, only conventional magnetic orders have been reported so far in isostructural Ce systems like, e. g., KCeO<sub>2</sub> [31], KCeS<sub>2</sub> [32–34], CsCeSe<sub>2</sub> [35, 36], with a possible exception of RbCeO<sub>2</sub> [37]. The effective spin-1/2 Hamiltonians of these delafossites remain rather uncertain due to the lack of single crystals, the high magnetic fields required to achieve full saturation, and the difficulty of unambiguously determining small anisotropic IEI from fitting magnetic excitations [11, 35]. Nevertheless, for several systems such experimental fits have been carried out [30, 33-35], in particular, for KCeS<sub>2</sub> [33, 34]and CsCeSe<sub>2</sub> [35, 36] that exhibit a simple quasi-collinear (yz-)stripe antiferromagnetic (AFM) order.

In spite of great interest in these systems, there have been only few attempts to elucidate their spin Hamiltonians theoretically [26, 34, 38]. Small NN anisotropies as well as next-nearest-neighbor (NNN) couplings with a typical magnitude below one Kelvin [11] are hard to reliably extract by direct total-energy DFT-based calculations. The magnitude of NNN superexchange calculated for Yb delafossites using DFT tight-binding 4f hopping is far too low to account for the putative QSL state and drastically disagrees with experimental estimates [38]. Two-site cluster calculations for KCeS<sub>2</sub> [34] predict reasonable IEI magnitudes and reproduce its yz-stripe order but do not account for some salient features of the excitation spectra.

Full spin Hamiltonians for a set of Ce delafossites were also calculated [26] using the force theorem in Hubbard-I (FT-HI) [15]. This method extracts all kinetic exchange couplings between localized shells of a correlated insulator from its paramagnetic electronic structure obtained using DFT+dynamical mean-field theory(DMFT) [39–

41] in conjunction with the quasi-atomic Hubbard-I (HI) approximation for on-site correlations [42]. The FT-HI approach has previously reliably described anisotropic and multipolar IEI in a number of transition metal, RE and actinide systems, see Ref. [18] for a review. However, in the case of Ce delafossites, the predicted IEI magnitude, though agreeing with experimental estimates for the oxides systems, appeared to be severely underestimated for the sulfide KCeS<sub>2</sub>, hinting at other coupling mechanisms beyond 4f kinetic exchange playing a key role in this compound.

Here, we generalize the FT-HI approach to include all indirect exchange contributions stemming from the 4f-5d on-site Coulomb repulsion. We first introduce this Coulomb interaction in its full form; treating it on a static mean-field level, we show that the FT-HI idea deriving IEI by considering the DFT+DMFT functional response to simultaneous fluctuations on two correlated shells in the paramagnetic phase – can be seamlessly extended to the 5d-mediated indirect exchange. Applying the generalized FT-HI to a set of Ce delafossites - the selenide CsCeSe<sub>2</sub>, sulfide KCeS<sub>2</sub>, and oxide RbCeO<sub>2</sub> we find a remarkable qualitative evolution of IEI. While the superexchange is found to dominate over the indirect exchange in the oxide, the situation is reversed in the selenide. Both coupling mechanisms are found to contribute comparably in the sulfide. The calculated IEI place  $CsCeSe_2$  and  $KCeS_2$  in the yz-stripe region of the published spin-1/2 triangular-lattice model phase diagram, in agreement with experiment, while those for  ${\rm RbCeO_2}$  correspond to the 120° AFM. We evaluate inelastic neutron scattering spectra for CsCeSe<sub>2</sub> and KCeS<sub>2</sub> finding that the calculated IEI provide a qualitative and quantitative agreement with single-crystal and polycrystalline data [34, 35] on a level comparable to the previously published experimental fits.

Generalized force theorem in Hubbard-I. We start by supplementing the one-electron Kohn-Sham Hamiltonian with on-site intra-shell ff and inter-shell fd Coulomb interactions

$$H = \sum_{\mathbf{k}\nu} \epsilon_{\mathbf{k}\nu} c_{\mathbf{k}\nu}^{\dagger} c_{\mathbf{k}\nu} + \sum_{i \in RE} H_{U,(i)}^{ff} + H_{U,(i)}^{fd} - H_{\mathrm{DC},(i)}, (1)$$

where  $c_{\mathbf{k}\nu}^{\dagger}$  creates the Bloch state  $\nu$  with energy  $\epsilon_{\mathbf{k}\nu}$  at the **k**-point in the Brillouin zone, the second sum is over all RE sites i. The four-index on-site ff and fd Coulomb repulsion  $H_U^{ff}=1/2\langle ab|U_{ff}|cd\rangle f_a^{\dagger}f_b^{\dagger}f_df_c$  and  $H_U^{fd}=\langle a\alpha|U_{fd}|b\beta\rangle f_a^{\dagger}d_{\alpha}^{\dagger}d_{\beta}f_b$  are defined in local f and d-shell correlated bases, where we label the f and d orbitals using a combined (Latin and Greek, respectively) spin-orbital index ( $a\equiv m_a^f\sigma_a^f$  etc.), summation over repeated indices is implied here and below.  $H_{\mathrm{DC},(i)}$  comprises double-counting correction terms for the 4f and 5d shells.

Within the DMFT framework, we use the HI approximation to treat the ff interaction between localized

4f orbitals, while the  $H_U^{fd}$  term involving dispersive 5d bands is mean-field decoupled, resulting in a static d-shell Hartree-Fork self-energy with matrix elements

$$\left[\Sigma^{\mathrm{HF},d}\right]_{\alpha\beta} = \left[\langle a\alpha|U_{fd}|b\beta\rangle - \langle a\alpha|U_{fd}|\beta b\rangle\right]\langle n_{ab}\rangle, \quad (2)$$

where  $n_{ab}=f_a^{\dagger}f_b,$  and an analogous term  $\Sigma^{\mathrm{HF},f}$  for the f-shell.

We assume that in the high-temperature paramagnetic phase modeled by DFT+HI, with the 4f shell localized due to the ff repulsion, the effect of  $H_U^{fd}$  is properly included on the static level within DFT.  $\Sigma^{\mathrm{HF}^{d(f)}}$  is thus fully compensated by the corresponding DC term in (1). This assumption is supported by a quantitatively good description of the CF splitting in the RE delafossites obtained in DFT+HI calculations without  $H_U^{fd}$  explicitly included [26], see also End Matter.

Subsequently, we focus on the 4f-shell GS multiplet (GSM), labeled by the (pseudo)angular momentum J, of dimension N=2J+1, with its states labeled by the projection M, and consider small fluctuations around its paramagnetic configuration. An on-site  $M_1M_2$  fluctuation is encoded as  $\epsilon\rho^{M_1M_2}$ , where  $\epsilon$  is a small parameter and  $\rho^{M_1M_2}$  is a traceless  $N\times N$  density matrix (DM) operator. Its matrix elements read  $\rho^{M_1M_2}_{MM'}=[\delta_{MM_1}\delta_{M'M_2}-\delta_{MM'}I/N]$ , where I is the unit matrix and the second term in the brackets compensates the change of the trace for diagonal fluctuations. In the FT-HI, matrix elements of the IEI Hamiltonian within the GSM manifold are obtained from the response of the DFT+DMFT grand potential  $\Omega$  [43, 44] to such fluctuations on two neighboring sites i and j:

$$\langle M_1^i M_3^j | H_{\text{IEI}} | M_2^i M_4^j \rangle = \frac{\delta^2 \Omega}{\delta \rho_i^{M_1 M_2} \delta \rho_j^{M_3 M_4}}.$$
 (3)

In the force-theorem spirit [45–47] only the kinetic-energy term in  $\Omega$  was shown [15] to contribute to (3) through the corresponding response of the on-site self-energy  $\delta \Sigma_i/\delta \rho_i$  (see End Matter for details).

In the generalized FT-HI, the  $\delta \Sigma_i/\delta \rho_i$  matrix consists of two diagonal ff and dd blocks given by  $\delta \Sigma_i^{\rm HI}/\delta \rho_i^{M_1M_2}$  and  $\delta \Sigma_i^{\rm HF,d}/\delta \rho_i^{M_1M_2}$ , respectively. The dynamical HI ff block was derived before [15]. To obtain the dd block we map the many-electron J-space DM  $\rho^{M_1M_2}$  into the 4f one-electron DM  $n_{ab}={\rm Tr}[n_{ab}^J\cdot \rho^{M_1M_2}]$ , where  $\left[n_{ab}^J\right]_{MM'}=\langle JM|f_a^\dagger f_b|JM'\rangle$  [48]. Substituting this into (2) we find

$$\delta \Sigma_{\alpha\beta}^{\mathrm{HF},d}/\delta \rho^{M_1 M_2} = \mathrm{Tr} \left[ U_{fd}^{J,\alpha\beta} \cdot \rho^{M_1 M_2} \right],$$
 (4)

where  $U_{fd}^{J,\alpha\beta} = \left[ \langle a\alpha | U_{fd} | b\beta \rangle - \langle a\alpha | U_{fd} | \beta b \rangle \right] n_{ab}^{J}$ .

The subsequent derivation is fully analogous to that of the original FT-HI, see Sec. IIB in Ref. [15], leading to the expression of the same form  $\langle M_1^i M_3^j | H_{\rm IEI} | M_2^i M_4^j \rangle = 1$ 

Tr 
$$\left[G_{ij} \frac{\delta \Sigma_j}{\delta \rho_j^{M_3 M_4}} G_{ji} \frac{\delta \Sigma_i}{\delta \rho_i^{M_1 M_2}}\right]$$
, where the trace is over the

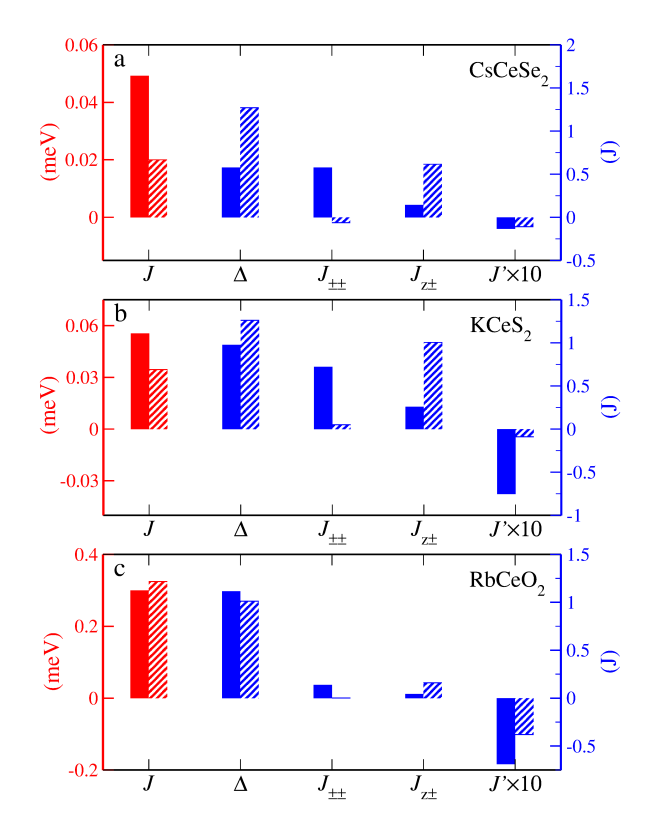


Figure 1: The calculated nearest-neighbor (NN) intersite exchange interaction J (in meV, left y-axis) together with the NN exchange anisotropy terms  $\Delta$ ,  $J_{\pm\pm}$ ,  $J_{z\pm}$ , and next-nearest-neighbor J' (in units of J, right y-axis) calculated by FT-HI method. The values obtained using the generalized FT-HI approach with the 5d-mediated indirect exchange included are shown as solid bars, whereas the hatched bars represent the superexchange-only values.

Matsubara frequencies (omitted for brevity), and orbital indices. However,  $\delta\Sigma/\delta\rho$  is now a block-diagonal matrix with its ff and dd blocks defined above. Correspondingly, the one-electron propagator matrix  $G_{ij}$  is composed of blocks  $[G_{ij}]_{bb'}=\mathrm{FT}_{ij}\left[P_{\mathbf{k},b}G_{\mathbf{k}}P_{\mathbf{k},b'}^{\dagger}\right]$ , where  $\mathrm{FT}_{ij}$  is the Fourier transform evaluated at the lattice vector  $\mathbf{R}_{ij}$ , b(b')=f,d are the block labels,  $P_{\mathbf{k},b}$  are the projectors to the corresponding correlated basis,  $G_{\mathbf{k}}$  is the DFT+HI lattice Green's function. One sees that the propagators  $[G_{ij}]_{bb'}$  include effective ff hopping leading to superexchange as well as the fd (df) and dd blocks that induce various indirect exchange contributions.

The generalized FT-HI approach is implemented in the framework of the "MagInt" code [49] using the TRIQS library [50, 51] and Wien2k linearized augmented-planewave (LAPW) DFT code [52].

Effective spin Hamiltonians and magnetic order. First, we carried self-consistent DFT+HI calculations to obtain the paramagnetic electronic structure and GS Kramers

doublet of the target compounds, see End Matter for details, and then computed their effective spin Hamiltonians using the generalized FT-HI.

The delafossites' structure symmetry constrains [22, 53–55] the most general IEI within the GS spin-1/2 manifold along the NN  $\mathbf{R}_{ij}$  bond x||[100] (see Fig. 2a) to the following form:

$$H_{ij} = \mathbf{S}_{i}^{T} \hat{J}_{ij} \mathbf{S}_{j} = J(\Delta S_{i}^{z} S_{j}^{z} + S_{i}^{x} S_{j}^{x} + S_{i}^{y} S_{j}^{y}) + 2J_{\pm\pm}(S_{i}^{x} S_{j}^{x} - S_{i}^{y} S_{j}^{y}) + J_{z\pm}(S_{i}^{z} S_{j}^{y} + S_{i}^{y} S_{j}^{z}),$$
(5)

where  $\mathbf{S} = [S^x, S^y, S^z]$ , the parameters  $\Delta$ ,  $J_{\pm\pm}$ , and  $J_{z\pm}$  determine the diagonal XXZ, diagonal XY and off-diagonal exchange anisotropy, respectively. The coupling  $\hat{J}'$  for the NNN bond along [010]||y takes the same form (5). The IEI for other NN and NNN bonds follow from the symmetry [26, 54, 55].

The key result of this work is shown in Fig. 1 where the IEI calculated by the generalized FT-HI are depicted together with the values obtained without the fd contribution, i. e. including the f - f superexchange (SE) only (the latter, for RbCeO<sub>2</sub> and KCeS<sub>2</sub>, closely agreeing with previous FT-HI results [26]). The difference between those two IEI sets is due to 5d-mediated f - f indirect exchange (dfIE). The dfIE contribution dominates in the selenide, whereas the dfIE and SE contribute almost equally in the sulfide. In the oxide, in contrast, the SE contribution is by far the most significant. Notably, the magnitude of the dfIE term remains comparable across all three systems, and the observed evolution is due to the SE magnitude strongly suppressed with decreasing electronegativity and increasing ionic radius along the chalcogen series  $O \rightarrow S \rightarrow Se$ . The impact of dfIE on the exchange anisotropy and long-distance NNN couplings remains significant even in RbCeO<sub>2</sub>. It is absolutely crucial in CsCeSe<sub>2</sub> and KCeS<sub>2</sub> changing the leading NN exchange anisotropy from the off-diagonal  $J_{z\pm}$  to the diagonal XY  $J_{\pm\pm}$  and, in KCeS<sub>2</sub>, also strongly enhancing the NNN coupling (see End Matter for the full list of calculated IEI).

Two physically distinct exchange processes contribute to the dfIE [2, 14]. The first one is generated by intershell  $H_U^{fd}$  on two RE sites mediated by dd virtual hopping, while the second one, mediated by fd hopping, occurs due to intrashell  $H_U^{ff}$  on one RE site and intershell  $H_U^{fd}$  on another one. The first process is thus RKKY-like involving no hopping from 4f-shell and previously analytically estimated to be negligible in Eu chalcogenides compared to the second one [2, 14]. In the generalized FT-HI we can single out the first process by setting the ff-block of  $\delta\Sigma/\delta\rho$  to zero. One can easily see that only dd hopping described by the corresponding propagator  $[G_{ij}]_{dd}$  contributes in this case. We find that the dd hopping-mediated process contributes overall about 10% of the total dfIE magnitude, its major part thus being due to fd virtual hopping.

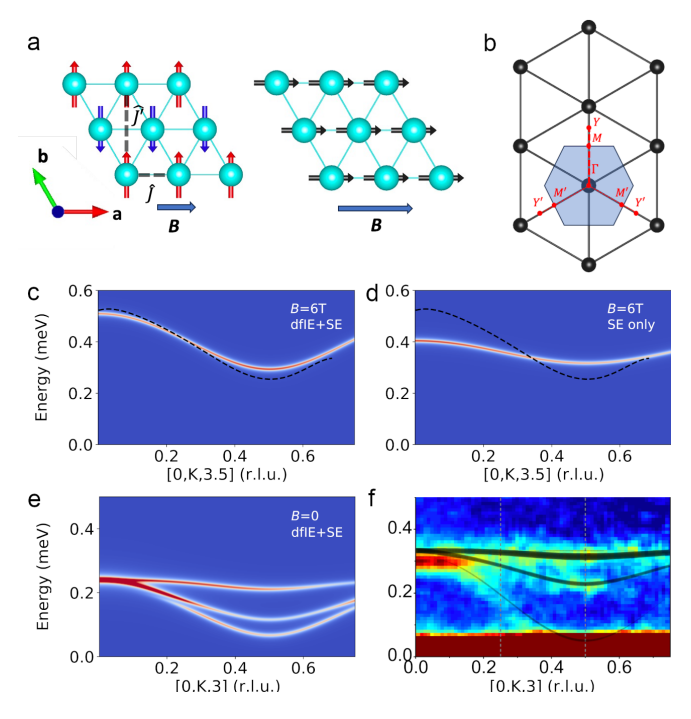


Figure 2: (a). Top view of the yz-stripe order (left) and the fully-polarized state (right). (b) Top view of the reciprocal triangular lattice. The first Brillouin zone is shaded, the  $K = \Gamma - M - Y$  path along which the INS in applied field is calculated is indicated by dashed red line, the thinner lines show the two equivalent  $\Gamma$  – M'-Y' paths. (c) The calculated INS intensity along the path [0, K, 3.5] in applied field of 6 Tesla using full IEI with the dfIE included. The experimental dispersion extracted from the experimental INS spectrum [35] at the same field is shown by the black dashed line. (d) The same data as in (c) calcualted using only SE IEI. (e) The zero-field INS calculated along [0, K, 3] using full IEI. (f). The experimental INS data at zero field [35]. The black lines were calculated with their experimental IEI fit. The figure is reproduced from Ref. [35] under CC-BY 4.0 license.

The GS magnetic phases corresponding to the calculated IEI can be inferred from published phase diagrams for the anisotropic triangular-lattice model [22, 23, 26, 55]. Both CsCeSe<sub>2</sub> and KCeS<sub>2</sub> lie deep within the region of yz-stripe AFM order (schematically depicted in Fig. 2a), owing to large diagonal  $J_{\pm\pm}$ , in agreement with experiment [33, 36]. The same order is actually stable with the SE-only IEI, but due to a different reason, namely, due to the off-diagonal exchange anisotropy  $J_{z\pm}$ . Finally, basing on the exact-diagonalization analysis of Ref. [26], RbCeO<sub>2</sub> is expected to be in the 120° AFM region owing to its relatively significant negative J', in spite of a report [37] finding no evidence for magnetic order in its thermodynamics.

Magnetic excitations. Magnetic excitations measured

with inelastic neutron scattering (INS) in CsCeSe<sub>2</sub> and KCeS<sub>2</sub> [34, 35] provide valuable data to test the calculated spin Hamiltonians. In particular, the INS experiment [35] in CsCeSe<sub>2</sub> was carried out in a single-crystal mode under applied field allowing to resolve excitations along different Brillouin-zone (BZ) directions. In small fields the yz-AFM is preserved, while in high fields of 5 T and above the system is in a fully-polarized (FP) ferromagnetic state (see Fig. 2a) featuring sharp magnon excitations.

In the high-field limit, magnetic excitations in CsCeSe<sub>2</sub> are expected to be reasonably well captured within simple approaches [35] like the random-phase approximation (RPA, see End Matter for details). To calculate CsCeSe<sub>2</sub> magnetic excitation spectra in RPA we first solved its effective Hamiltonian within a single-site mean-field (MF) approximation [56] applying the field along the a direction. In zero field we obtained the expected yz-stripe order with a small out-of-plane component,  $|\langle S^y \rangle| = 0.50$ and  $|\langle S^z \rangle| = 0.06$ . The calculated in-plane ordered moment  $0.98\mu_B$  is significantly overestimated compared to the neutron diffraction value of  $0.65\mu_B$ , though agreeing reasonably well with experimental INS estimate (0.88)  $\mu_B$ ) [35, 36]. This suggests strong fluctuations reducing the ordered moment with respect to its "atomic" MF value.

With such effects being beyond a simple MF-RPA treatment, we mainly focus on comparing calculated excitations in CsCeSe<sub>2</sub> at high fields. Since experimentally the Ce local moment appears to be field-dependent even in the FP phase [36], we compare the measured [35] and calculated INS data at the applied field of 6 Tesla, at which the experimental value of the in-plain moment [36] coincides with our quasi-atomic value of 0.98  $\mu_B$  to have the same field-dependent shift. In the fully-aligned FP state, the spin-wave dispersion is independent of this shift [57]. We obtain a very good quantitative agreement with experimental dispersion (Fig. 2c) along the  $\Gamma - M - Y$  path in the reciprocal space (sketched in Fig. 2b) when the full calcualted IEI including the dfIE contribution are used.

Without dfIE, i. e., with only the SE included, the GS magnetic order is still yz-stripe, but with a large z-component of the ordered moment ( $|\langle S_z \rangle|$ =0.35). The dispersion in the FP state is strongly underestimated (Fig. 2d).

In order to evaluate magnetic excitations at zero field along the same  ${\bf q}$ -path, we summed up the contributions the for three equivalent paths in the reciprocal space shown in Fig. 2b to account for equally populated domains of the yz-order. The resulting theoretical INS (Fig 2e) is in good qualitative agreement with the experimental one (Fig 2f) albeit with the excitation energies underestimated by about 25% compared to experiment.

We apply the same approach to calculate INS intensity in KCeS<sub>2</sub>. Solving the full dfIE+SE Hamiltonian within

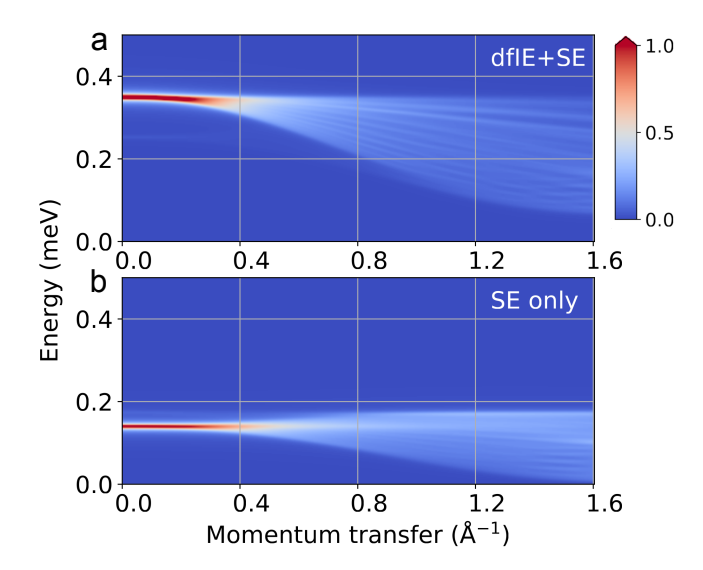


Figure 3: (a). Spherically-averaged INS intensity of KCeS<sub>2</sub> calculated using the full IEI Hamiltonian with the dfIE included (a) and using the superexchange IEI only (b).

MF results, similarly to CsCeSe<sub>2</sub>, in an yz-order with a nearly in-plane moment direction  $(|\langle S^y \rangle| = 0.49)$  and  $|\langle S^z \rangle| = 0.09$ . The calculated spherically averaged INS intensity (Fig. 3a) features a sharp quasi-dispersionless branch at about 0.35 meV for q < 0.3 Å<sup>-1</sup>, which spreads into a broad diffusive feature from 10 to 35 meV at q > 1.2 Å<sup>-1</sup>; this picture agrees quite well qualitatively and quantitatively with the experimental low-T INS data [34]. Neglecting the dfIE contribution we find in MF, analogously to CsCeSe<sub>2</sub>, a yz-order with a large out-of-plane component ( $|\langle S_z \rangle| = 0.36$ ). The corresponding INS spectra (Fig. 3b) features the high-intensity branch at an energy that is about half the experimental value.

Outlook. The generalized FT-HI method introduced in this Letter is not, per se, limited to insulators and remains applicable as long as the correlated f-shell is localized. A wide range of applications is hereby possible, including RE metals and local-moment RE intermetallics, localized actinide systems, as well as other RE insulating systems, like the highly frustrated RE pyrochlores. The method can be straightforwardly extended to multiple itinerant shells coupled through an on-site intershell Coullomb interaction to the localized quasi-atomic 4f one, e. g., both the RE 5d and 6s shell can be included simultaneously. The 4f-6s Hund's rule interaction was recently shown to be sizable [58]. An important advantage of the method is its ability to separately evaluate the contributions of various exchange mechanisms, while employing the same framework and the same set of correlated orbitals. The limitation of its present implementation is that an experimental input is required to define  $U_{fd}$  (though the most material sensitive parameter  $F^0$  is irrelevant). Combining the generalized FT-HI with *ab initio* determination of the f-d on-site interaction, like the constrained RPA method [59], is, therefore, a promising avenue for its future development.

Acknowledgments. The author is grateful to Dario Fiore Mosca for useful discussions and to the CPHT computer team for support.

- \* leonid.poyurovskiy@polytechnique.edu
- J. Jensen and A. R. Mackintosh, Rare Earth Magnetism: Structures and Excitations (Clarendon Press, Oxford, 1991).
- [2] A. Mauger and C. Godart, Physics Reports 141, 51 (1986).
- [3] R. Shiina, H. Shiba, and P. Thalmeier, Journal of the Physical Society of Japan 66, 1741 (1997), https://doi.org/10.1143/JPSJ.66.1741.
- [4] A. S. Cameron, G. Friemel, and D. S. Inosov, Reports on Progress in Physics 79, 066502 (2016).
- [5] P. Santini, S. Carretta, G. Amoretti, R. Caciuffo, N. Magnani, and G. H. Lander, Rev. Mod. Phys. 81, 807 (2009).
- [6] S. Khmelevskyi and L. V. Pourovskii, Communications Physics 7, 12 (2024).
- [7] T. Onimaru and H. Kusunose, Journal of the Physical Society of Japan 85, 082002 (2016).
- [8] M. J. P. Gingras and P. A. McClarty, Reports on Progress in Physics 77, 056501 (2014).
- [9] R. Sibille, N. Gauthier, E. Lhotel, V. Porée, V. Pomjakushin, R. A. Ewings, T. G. Perring, J. Ollivier, A. Wildes, C. Ritter, T. C. Hansen, D. A. Keen, G. J. Nilsen, L. Keller, S. Petit, and T. Fennell, Nature Physics 16, 546 (2020).
- [10] E. M. Smith, E. Lhotel, S. Petit, and B. D. Gaulin, Annual Review of Condensed Matter Physics 16, 387 (2025).
- [11] M. Xie, W. Zhuo, Y. Cai, Z. Zhang, and Q. Zhang, Chinese Physics Letters 41, 117505 (2024).
- [12] T. Arh, B. Sana, M. Pregelj, P. Khuntia, Z. Jagličić, M. D. Le, P. K. Biswas, P. Manuel, L. Mangin-Thro, A. Ozarowski, and A. Zorko, Nature Materials 21, 416 (2022).
- [13] B. Johansson, The Philosophical Magazine: A Journal of Theoretical Experimental and Applied Physics 30, 469 (1974).
- [14] T. Kasuya, IBM Journal of Research and Development 14, 214 (1970).
- [15] L. V. Pourovskii, Phys. Rev. B 94, 115117 (2016).
- [16] N. Iwahara, Z. Huang, I. Neefjes, and L. F. Chibotaru, Phys. Rev. B 105, 144401 (2022).
- [17] J. Otsuki, K. Yoshimi, H. Shinaoka, and H. O. Jeschke, Phys. Rev. B 110, 035104 (2024).
- [18] L. V. Pourovskii, D. Fiore Mosca, L. Celiberti, S. Khmelevskyi, A. Paramekanti, and C. Franchini, Nature Reviews Materials 10, 674 (2025).
- [19] Z. Zhu and S. R. White, Phys. Rev. B 92, 041105 (2015).
- [20] Y. Iqbal, W.-J. Hu, R. Thomale, D. Poilblanc, and F. Becca, Phys. Rev. B 93, 144411 (2016).
- [21] W.-J. Hu, S.-S. Gong, W. Zhu, and D. N. Sheng, Phys. Rev. B 92, 140403 (2015).

- [22] Z. Zhu, P. A. Maksimov, S. R. White, and A. L. Chernyshev, Phys. Rev. Lett. 120, 207203 (2018).
- [23] M. Wu, D.-X. Yao, and H.-Q. Wu, Phys. Rev. B 103, 205122 (2021).
- [24] N. E. Sherman, M. Dupont, and J. E. Moore, Phys. Rev. B 107, 165146 (2023).
- [25] A. Wietek, S. Capponi, and A. M. Läuchli, Phys. Rev. X 14, 021010 (2024).
- [26] L. V. Pourovskii, R. D. Soares, and A. Wietek, Ab initio spin hamiltonians and magnetism of ce and yb triangular-lattice compounds (2025), arXiv:2509.03177 [cond-mat.str-el].
- [27] M. M. Bordelon, E. Kenney, C. Liu, T. Hogan, L. Posthuma, M. Kavand, Y. Lyu, M. Sherwin, N. P. Butch, C. Brown, M. J. Graf, L. Balents, and S. D. Wilson, Nature Physics 15, 1058 (2019).
- [28] R. Sarkar, P. Schlender, V. Grinenko, E. Haeussler, P. J. Baker, T. Doert, and H.-H. Klauss, Phys. Rev. B 100, 241116 (2019).
- [29] P.-L. Dai, G. Zhang, Y. Xie, C. Duan, Y. Gao, Z. Zhu, E. Feng, Z. Tao, C.-L. Huang, H. Cao, A. Podlesnyak, G. E. Granroth, M. S. Everett, J. C. Neuefeind, D. Voneshen, S. Wang, G. Tan, E. Morosan, X. Wang, H.-Q. Lin, L. Shu, G. Chen, Y. Guo, X. Lu, and P. Dai, Phys. Rev. X 11, 021044 (2021).
- [30] A. O. Scheie, Y. Kamiya, H. Zhang, S. Lee, A. J. Woods, M. O. Ajeesh, M. G. Gonzalez, B. Bernu, J. W. Villanova, J. Xing, Q. Huang, Q. Zhang, J. Ma, E. S. Choi, D. M. Pajerowski, H. Zhou, A. S. Sefat, S. Okamoto, T. Berlijn, L. Messio, R. Movshovich, C. D. Batista, and D. A. Tennant, Phys. Rev. B 109, 014425 (2024).
- [31] M. M. Bordelon, X. Wang, D. M. Pajerowski, A. Banerjee, M. Sherwin, C. M. Brown, M. S. Eldeeb, T. Petersen, L. Hozoi, U. K. Rößler, M. Mourigal, and S. D. Wilson, Phys. Rev. B 104, 094421 (2021).
- [32] G. Bastien, B. Rubrecht, E. Haeussler, P. Schlender, Z. Zangeneh, S. Avdoshenko, R. Sarkar, A. Alfonsov, S. Luther, Y. A. Onykiienko, H. C. Walker, H. Kühne, V. Grinenko, Z. Guguchia, V. Kataev, H. H. Klauss, L. Hozoi, J. van den Brink, D. S. Inosov, B. Büchner, A. U. B. Wolter, and T. Doert, SciPost Phys. 9, 041 (2020).
- [33] A. A. Kulbakov, S. M. Avdoshenko, I. Puente-Orench, M. Deeb, M. Doerr, P. Schlender, T. Doert, and D. S. Inosov, Journal of Physics: Condensed Matter 33, 425802 (2021).
- [34] S. M. Avdoshenko, A. A. Kulbakov, E. Häußler, P. Schlender, T. Doert, J. Ollivier, and D. S. Inosov, Phys. Rev. B 106, 214431 (2022).
- [35] T. Xie, S. Gozel, J. Xing, N. Zhao, S. M. Avdoshenko, L. Wu, A. S. Sefat, A. L. Chernyshev, A. M. Läuchli, A. Podlesnyak, and S. E. Nikitin, Phys. Rev. Lett. 133, 096703 (2024).
- [36] T. Xie, N. Zhao, S. Gozel, J. Xing, S. M. Avdoshenko, K. M. Taddei, A. I. Kolesnikov, L. D. Sanjeewa, P. Ma, N. Harrison, C. dela Cruz, L. Wu, A. S. Sefat, A. L. Chernyshev, A. M. Läuchli, A. Podlesnyak, and S. E. Nikitin, Phys. Rev. B 110, 054445 (2024).
- [37] B. R. Ortiz, M. M. Bordelon, P. Bhattacharyya, G. Pokharel, P. M. Sarte, L. Posthuma, T. Petersen, M. S. Eldeeb, G. E. Granroth, C. R. Dela Cruz, S. Calder, D. L. Abernathy, L. Hozoi, and S. D. Wilson, Phys. Rev. Mater. 6, 084402 (2022).
- [38] J. W. Villanova, A. O. Scheie, D. A. Tennant,

- S. Okamoto, and T. Berlijn, Phys. Rev. Res. **5**, 033050 (2023).
- [39] A. Georges, G. Kotliar, W. Krauth, and M. J. Rozenberg, Rev. Mod. Phys. 68, 13 (1996).
- [40] V. I. Anisimov, A. I. Poteryaev, M. A. Korotin, A. O. Anokhin, and G. Kotliar, Journal of Physics: Condensed Matter 9, 7359 (1997).
- [41] A. I. Lichtenstein and M. I. Katsnelson, Phys. Rev. B 57, 6884 (1998).
- [42] J. Hubbard, Proc. Roy. Soc. (London) A 276, 238 (1963).
- [43] G. Kotliar, S. Y. Savrasov, K. Haule, V. S. Oudovenko, O. Parcollet, and C. A. Marianetti, Rev. Mod. Phys. 78, 865 (2006).
- [44] A. Georges, AIP Conference Proceedings **715**, 3 (2004).
- [45] A. R. Mackintosh and O. Andersen (Cambridge University Press, 1980) Chap. The electronic structure of transition metals.
- [46] A. Liechtenstein, M. Katsnelson, V. Antropov, and V. Gubanov, Journal of Magnetism and Magnetic Materials 67, 65 (1987).
- [47] A. Szilva, Y. Kvashnin, E. A. Stepanov, L. Nordström, O. Eriksson, A. I. Lichtenstein, and M. I. Katsnelson, Rev. Mod. Phys. 95, 035004 (2023).
- [48] D. Fiore Mosca, L. V. Pourovskii, and C. Franchini, Phys. Rev. B 106, 035127 (2022).
- [49] L. V. Pourovskii and D. Fiore Mosca, MagInt, https://github.com/MagInteract/MagInt.
- [50] O. Parcollet, M. Ferrero, T. Ayral, H. Hafermann, I. Krivenko, L. Messio, and P. Seth, Computer Physics Communications 196, 398 (2015).
- [51] M. Aichhorn, L. V. Pourovskii, P. Seth, V. Vildosola, M. Zingl, O. E. Peil, X. Deng, J. Mravlje, G. J. Kraberger, C. Martins, et al., Computer Physics Communications 204, 200 (2016).
- [52] P. Blaha, K. Schwarz, G. Madsen, D. Kvasnicka, J. Luitz, R. Laskowski, F. Tran, and L. D. Marks, WIEN2k, An augmented Plane Wave + Local Orbitals Program for Calculating Crystal Properties (Karlheinz Schwarz, Techn. Universität Wien, Austria, ISBN 3-9501031-1-2, 2018).
- [53] Y. Li, G. Chen, W. Tong, L. Pi, J. Liu, Z. Yang, X. Wang, and Q. Zhang, Phys. Rev. Lett. 115, 167203 (2015).
- [54] J. Iaconis, C. Liu, G. B. Halász, and L. Balents, SciPost Phys. 4, 003 (2018).
- [55] P. A. Maksimov, Z. Zhu, S. R. White, and A. L. Chernyshev, Phys. Rev. X 9, 021017 (2019).
- [56] M. Rotter, Journal of Magnetism and Magnetic Materials 272-276, E481 (2004), proceedings of the International Conference on Magnetism (ICM 2003).
- [57] Y.-D. Li, Y. Shen, Y. Li, J. Zhao, and G. Chen, Phys. Rev. B 97, 125105 (2018).
- [58] M. Pivetta, F. m. c. Patthey, I. Di Marco, A. Subramonian, O. Eriksson, S. Rusponi, and H. Brune, Phys. Rev. X 10, 031054 (2020).
- [59] F. Aryasetiawan, M. Imada, A. Georges, G. Kotliar, S. Biermann, and A. I. Lichtenstein, Phys. Rev. B 70, 195104 (2004).
- [60] T. Plefka, Journal of Physics A: Mathematical and General 15, 1971 (1982).
- [61] A. Georges and J. S. Yedidia, Journal of Physics A: Mathematical and General 24, 2173 (1991).
- [62] M. Aichhorn, L. V. Pourovskii, V. Vildosola, M. Ferrero, O. Parcollet, T. Miyake, A. Georges, and S. Biermann, Phys. Rev. B 80, 085101 (2009).

- [63] L. V. Pourovskii, J. Boust, R. Ballou, G. G. Eslava, and D. Givord, Phys. Rev. B 101, 214433 (2020).
- [64] R. Cowan, The Theory of Atomic Structure and Spectra, Los Alamos Series in Basic and Applied Sciences (University of California Press, 1981).
- [65] G. W. Burdick and M. F. Reid, in *Handbook on the Physics and Chemistry of Rare Earths*, Vol. 37, edited by K. A. Gschneidner, J.-C. Bünzli, and V. K. Pecharsky (Elsevier, 2007) pp. 61–98.
- [66] P. Delange, S. Biermann, T. Miyake, and L. Pourovskii, Phys. Rev. B 96, 155132 (2017).
- [67] S. W. Lovesey and G. van der Laan, Phys. Rev. B 101, 144419 (2020).

## END MATTER

## Outline of FT-HI approach

In order to render this paper self-contained, we briefly outline the FT-HI approach [15] here. We start by assuming the following form for the low-energy effective quantum Hamiltonian of the system:

$$H_{\text{eff}} = H_{1s} + H_{\text{IEI}} = H_{1s} + \sum_{\langle ij \rangle} \sum_{\alpha\beta} V_{ij}^{\alpha\beta} O^{\alpha}(i) O^{\beta}(j), (6)$$

where  $H_{1s}$  is the one-site (typically, crystal field) term,  $H_{\rm IEI}$  is the two-site IEI one,  $O^{\alpha}(i)$  are operators encoding degrees of freedom within the GSM of a given site and labeled by an index  $\alpha$ . The GSM is labeled by (pseudo)-angular momentum J and spanned by its  $|JM\rangle$  eigenstates, with M=-J,-J+1,...,J. The operators  $O^{\alpha}$  are traceless thus conserving the total GSM occupancy, but otherwise their form is arbitrary (they can be angular momentum operators, Stevens operators, spherical tensors etc.). In this section we abbreviate  $|JM_1\rangle$  at site i as  $|1_i\rangle$ . Hereby, two-site matrix elements of (6) read

$$\langle 1_i 3_j | H_{\text{IEI}} | 2_i 4_j \rangle = \sum_{\alpha\beta} V_{ij}^{\alpha\beta} O_{12}^{\alpha} O_{34}^{\beta}. \tag{7}$$

Using the operators  $\rho^{M_1M_2} \equiv \rho^{12}$  introduced in the main text, any traceless operator  $O^{\alpha}$  can be trivially written as  $\sum_{12} O^{\alpha}_{12} \rho^{12}$ . Inserting this into  $H_{\rm IEI}$  and using (7) one finds:

$$H_{\rm IEI} = \sum_{\langle ij\rangle} \sum_{1234} \langle 1_i 3_j | H_{\rm IEI} | 2_i 4_j \rangle \rho_i^{12} \rho_j^{34}.$$

The mean-field free energy  $\Omega_{\rm MF}$  of (6) for a chosen set of expectation values of all  $\rho$  at all sites then reads [44, 60, 61]:

$$\Omega_{\rm MF} = \Omega_{1s} + \sum_{\langle ij \rangle} \sum_{1234} \langle 1_i 3_j | H_{\rm IEI} | 2_i 4_j \rangle \langle \rho_i^{12} \rangle \langle \rho_j^{34} \rangle,$$

where the first term comprises single-site entropic and energetic contributions and the second term is the mean-field total energy contribution due to the 2-site term. Therefore the response to two-site fluctuation of  $\rho$  is given by the corresponding matrix element of the two-site Hamiltonian:

$$\frac{\delta^2\Omega_{\rm MF}}{\delta\rho_i^{12}\delta\rho_j^{34}} = \langle 1_i 3_j | H_{\rm IEI} | 2_i 4_j \rangle.$$

If the low-energy physics of the system is represented by (6) then its full electronic model including all energy scales and solved within a (dynamical) mean-field approximation should have the same response,  $\frac{\delta^2 \Omega_{\rm MF}}{\delta \rho_i^{12} \delta \rho_j^{34}} = \frac{\delta^2 \Omega_{\rm DFT+DMFT}}{\delta \rho_i^{12} \delta \rho_j^{34}}$ , from which eq. 3 of the main text follows.

In order to evaluate  $\frac{\delta^2 \Omega_{\mathrm{DFT}+\mathrm{DMFT}}}{\delta \rho_i^{12} \delta \rho_j^{34}}$ , Ref. [15] employs a force theorem approach evaluating the response of the kinetic energy term in  $\Omega_{\mathrm{DFT}+\mathrm{DMFT}}$  only. The latter is given by  $\frac{1}{\beta}\mathrm{Tr}\ln\left[G_{\mathrm{latt}}^{\mathbf{k},n}\right]=-\frac{1}{\beta}\mathrm{Tr}\ln\left[i\omega_n+\mu-H_{\mathrm{KS}}-P_{\mathbf{k}}^{\dagger}(\Sigma(i\omega_n)-\Sigma_{\mathrm{DC}})P_{\mathbf{k}}\right]$ , where  $\omega_n$  is the fermionic Matsubara frequency,  $\mu$  is the chemical potential,  $H_{\mathrm{KS}}$  is the Kohn-Sham Hamiltonian,  $\Sigma_{\mathrm{DC}}$  is the self-energy double counting term, other quantities are defined in the main text. Within the force-theorem approximation, only the same-site self-energy  $\Sigma_i(i\omega_n)$  is affected by a fluctuation in  $\rho_i$  leading to the FT-HI equation for  $\langle 1_i 3_j | H_{\mathrm{IEI}} | 2_i 4_j \rangle$  that is given in the main text.

## DFT+HI calculations

We calculated all three compounds in DFT+HI using their experimental lattice structures [33, 36, 37] employing the Wien2k linearized augmented-plane-wave (LAPW) code [52], TRIQS library implementation of DFT+DMFT [50, 51] and the Hubbard-I implementation provided by the MagInt package [49]. In those DFT+HI calculations we employ 1000 k-points in the full Brillouin zone, the LAPW basis cutoff  $R_{\rm MIN}K_{\rm MAX}{=}8$ , the spin-orbit coupling is included through the standard second-variation approach, the LDA is used as the DFT exchange-correlation potential. The double counting correction is calculated in accordance with the fully-localized-limit formula using the nominal occupancy  $f^1$ .

The projected Wannier correlated bases [62] were constructed using the same "large" ([-9.5:9.5] eV, for X-p and Ce-5d) and the "small" ([-1.63:1.56] eV for Ce-4f) energy windows for all 3 compounds, the latter window chosen such as to include 4f only excluding the rest in order to properly account for hybridization contribution to the crystal field splitting [63]. The resulting full set of Ce 5d, Ce 4f, and X p correlated orbitals is then orthonormalized using the standard prescription of the projective construction approach [62] to obtain a proper Wannier basis.

We specified the rotationally invariant ff Coulomb vertex using the standard values  $F^0 = U = 6$  eV and  $J_H = 0.7$  eV for Ce<sup>3+</sup> that were also used in Ref. [26]. The fd rotationally invariant Coulomb vertex was defined [64] using the Slater integrals values  $F^2 = 2.82$ ,  $F^4 = 1.40$ ,  $G^1 = 1.20$ ,  $G^3 = 1.04$ , and  $G^5 = 0.81$  eV extracted from optical measurements of  $4f^2 \rightarrow 4f^15d^1$  excitations in  $\Pr^{3+}$  doped in LiYF<sub>4</sub> host [65]. The use of  $\Pr^{3+}$  fd Slater parameters for Ce<sup>3+</sup> is justified by those parameters being basically constant between  $\Pr^{3+}$  and  $\operatorname{Nd}^{3+}$  with the change  $\lesssim 1\%$  [65]. We note that the fd Slater parameter  $F^0$ , which is expected to be strongly system dependent, does not contribute to (4) since the

fluctuations  $\delta \rho^{M_1 M_2}$  conserve the 4f shell occupancy.

Our self-consistent DFT+HI calculations were carried out employing the averaging over the  ${}^2F_{5/2}$  GSM of Ce  $4f^1$  to suppress the unphysical DFT self-interaction contribution to CF [66]. The calculated CF splitting and GS doublet agree rather well with experimental estimates [33, 36, 37]. However, as in Ref. [26], we do not reproduce the "superfluous" third CF mode experimentally observed in all three systems. This mode cannot be explained within a single-ion CF model, see, e. g., Refs. [33, 36, 37]. In CsCeSe<sub>2</sub>, we find a strong in-plane anisotropy of the GS g-tensor with in-plane  $g_x = g_y = 1.96$  and out-of plane  $g_z = -0.20$  agreeing with the range of values obtained by different experimental probes [35, 36], see Table I for the CF splitting and eigenstates in CsCeSe<sub>2</sub>. The calculated CF splittings in KCeS<sub>2</sub> and RbCeO<sub>2</sub> are the same as reported in Ref. [26] apart from minute differences due to slight changes in the 4fcorrelated basis.

#### Intersite exchange interactions

The IEI interaction  $\hat{J}_{ij}$  in the spin-1/2 Hamiltonian (5) is obtained from the FT-HI-calculated matrix elements  $\langle M_1^i M_3^j | H_{\rm IEI} | M_2^i M_4^j \rangle$  as follows:

$$J_{ij}^{pp'} = 2\langle M_1^i M_3^j | H_{\rm IEI} | M_2^i M_4^j \rangle S_{M_2 M_1}^p S_{M_4 M_3}^{p'},$$

where  $S^{p(p')}$  are the spin-1/2 operators, p(p') = x, y, z, the prefactor 2 stems from the spin-1/2 operators' normalization.

In Table II we list the calculated full IEI interactions, with indirect exchange included, for the NN bond along the x axis and the NNN bond along the y axis, see Fig. 2a. Apart from the NN anisotropy, we include also the full NNN anisotropy. To distinguish the NN and NNN parameters, the latter are primed  $(J', \Delta' \text{ etc.})$ . We also list the average value,  $J^{\text{int}} = Tr[\hat{J}^{\text{int}}]/3$ , for the shortest interlayer coupling.

$\overline{E}$	Wavefunction		
0	$0.884 5/2;\mp1/2\rangle\pm0.466 5/2;\pm5/2\rangle-0.037 7/2;\mp7/2\rangle$		
38	$\begin{array}{c} 0.995 5/2;\pm 3/2\rangle \mp 0.073 5/2;\mp 3/2\rangle \mp 0.060 7/2;\pm 3/2\rangle \\ +0.040 7/2;\mp 3/2\rangle \end{array}$		
60	$0.881 5/2;\pm 5/2\rangle \mp 0.463 5/2;\mp 1/2\rangle \pm 0.068 7/2;\mp 7/2\rangle \\ +0.067 7/2;\mp 1/2\rangle$		

Table I: Calculated CF energies E (in meV) and CF Kramers doublets wavefunctions in CsCeSe<sub>2</sub>.

	CaCaCa	I/CoC	Dh.CaO
	$CsCeSe_2$	$KCeS_2$	$RbCeO_2$
J  (meV)	0.049	0.055	0.299
$\Delta$	0.574	0.971	1.110
$J_{\pm\pm}/J$	0.572	0.717	0.133
$ J_{z\pm}/J $	0.138	0.254	0.040
J'/J	-0.013	-0.075	-0.069
$\Delta'$	3.548	0.555	0.640
$J'_{\pm\pm}/J'$	-1.710	-0.207	-0.018
$ J_{z\pm}'/J' $	1.517	0.181	0.115
$J^{^{ m int}}/J$	-0.008	-0.027	-0.036

Table II: Calculated IEI with indirect exchange included.

#### INS intensity calculations within RPA

The INS intensity at the energy E and momentum  ${\bf q}$  reads

$$I(\mathbf{q}, E) = F^{2}(|\mathbf{q}|) \sum_{\substack{pp'\\ij'}} \left( \delta_{pp'} - \frac{q_{p}q_{p'}}{q^{2}} \right) g_{p}g_{p'} \operatorname{Im} \chi_{pp'}^{ii'}(\mathbf{q}, E),$$

where  $F(|\mathbf{q}|)$  is the Ce<sup>3+</sup> form factor in the dipole approximation.  $\chi(\mathbf{q}, E)$  is the dynamical susceptibility, p and p' = x, y, z, i and i' run over the sites of the magnetic unit cell. We evaluate the dynamical susceptibility  $\chi(\mathbf{q}, E)$  using the usual RPA formula (for a general introduction into the RPA and its application to magnetic excitations see, e. g., Ref. [1]) that reads

$$\bar{\chi}^{-1}(\mathbf{q}, E) = \bar{\chi}_0^{-1}(E) + \bar{J}_{\mathbf{q}},$$

where  $\chi_0(E)$  is the single-site susceptibility evaluated from the on-site mean-field potential in the ordered phase,  $J_{\mathbf{q}}$  is the Fourier-transformed calculated IEI, the bar labels matrices in the p and i indices. The Ce<sup>3+</sup> form-factor  $F(|\mathbf{q}|)$  was calculated in accordance with the standard formula employing the radial integrals  $\langle j_0(q) \rangle$  and  $\langle j_2(q) \rangle$  obtained in Ref. [67] using a relativistic Hartree-Fock approach [64].

In order to simulate polycrystalline INS data in KCeS<sub>2</sub> we average, for each  $q=|\mathbf{q}|$ , the intensity  $I(\mathbf{q},E)$  as  $I(q,E)=\sum_{\mathbf{q},|\mathbf{q}|=q}I(\mathbf{q},E)$  over an equidistant spherical **q**-mesh containing 642 **q**-points.